The Astrophysical Journal, 818:127 (8pp), 2016 February 20 doi:10.3847/0004-637X/818/2/127

ACTIVE LONGITUDE AND SOLAR FLARE OCCURRENCES

N. Gyenge[1,2], A. Ludmány[1], and T. Baranyi[1]
[1] Debrecen Heliophysical Observatory (DHO), Konkoly Observatory, Research Centre for Astronomy and Earth Sciences, Hungarian Academy of Sciences Debrecen, P.O.Box 30, H-4010, Hungary; gyenge.norbert@csfk.mta.hu
[2] Solar Physics and Space Plasmas Research Centre (SP2RC), School of Mathematics and Statistics, University of Sheffield, Hounsfield Road, Hicks Building, Sheffield S3 7RH, UK
Received 2015 July 29; accepted 2015 December 23; published 2016 February 16

ABSTRACT

The aim of the present work is to specify the spatio-temporal characteristics of flare activity observed by the *Reuven Ramaty High Energy Solar Spectroscopic Imager* (*RHESSI*) and the *Geostationary Operational Environmental Satellite* (*GOES*) in connection with the behavior of the longitudinal domain of enhanced sunspot activity known as active longitude (AL). By using our method developed for this purpose, we identified the AL in every Carrington Rotation provided by the Debrecen Photoheliographic Data. The spatial probability of flare occurrence has been estimated depending on the longitudinal distance from AL in the northern and southern hemispheres separately. We have found that more than 60% of the *RHESSI* and *GOES* flares is located within $\pm 36^\circ$ from the AL. Hence, the most flare-productive active regions tend to be located in or close to the active longitudinal belt. This observed feature may allow for the prediction of the geo-effective position of the domain of enhanced flaring probability. Furthermore, we studied the temporal properties of flare occurrence near the AL and several significant fluctuations were found. More precisely, the results of the method are the following fluctuations: 0.8, 1.3, and 1.8 years. These temporal and spatial properties of the solar flare occurrence within the active longitudinal belts could provide us with an enhanced solar flare forecasting opportunity.

Key words: Sun: activity – Sun: flares – sunspots

1. INTRODUCTION

The spatial distribution and temporal behavior of flare occurrences are important elements of space weather. Regarding spatial properties, the latitudinal distribution (i.e., the butterfly diagram) is easily detectable because it is connected to the well-known varying latitude of the activity during the solar cycle. The determination of the longitudinal distribution is a harder challenge. It was mentioned as early as in the 19th century by Carrington (1863) that sunspot groups may prefer some longitudinal domains. This was also observed later by Maunder (1905) and Losh (1939). In the following decades, it was usually considered that sunspot emergence was not equally probable at all heliographic longitudes, but the results of localization attempts were not always convincing. The causes of the differing results are diverse.

Two approaches were followed. One of them considered the locations of enhanced activity to be "active nests" as isolated entities of the activity in the works of Becker (1955), Brouwer & Zwaan (1990), and Castenmiller et al. (1986). The other approach addresses active longitudes (hereafter AL) as persistent domains of activity. The presumptions of the applied methods are different and they may have a considerable impact on the results. Possible presumptions are the following: a rigidly rotating frame carrying an active longitudinal domain as reported by Balthasar & Schüssler (1983), Kitchatinov & Olemskoy (2005), and Ivanov (2007); persistent ALs under the influence of differential rotation presented, e.g., by Usoskin et al. (2005) and Zhang et al. (2011a); two ALs at a distance of 180° as in Usoskin et al. (2005). There were also skeptic views: Pelt et al. (2005) showed that some results may be artefacts of the applied methods, Henney & Durney (2005) even questioned the existence of ALs.

The preferred longitudinal domains of flares have been studied with similar presumptions and methods to those of the sunspot studies. The active nests are called "superactive regions" (Bai 1987) or "hot spots" (Bai 1988). The idea of rigid rotation also arises (Warwick 1965), but the obtained rotation rates are diverse (Bai 2003). The role of differential rotation is also considered and the presumption of the twin ALs at 180° apart (Zhang et al. 2007, 2011b). It seems reasonable to study the ALs of sunspots and flares together.

In our previous paper (Gyenge et al. 2014, hereafter Paper I), we endeavoured to follow procedure that was presumption-free, reasonable, and possible. The activity concentration has been computed for each longitudinal stripe of 10° in each Carrington rotation (CR) and all of these longitudinal distributions have been plotted in a time-longitude diagram. The migration of the positions of strongest concentrations in the time-longitude domain outlined a forward–backward motion of the most active longitudinal domain with respect to the Carrington frame. The half width of this AL was about 30°, a flip-flop event was identified, but the most interesting result was that the flux emergence exhibited a 1.3-year periodicity within the active longitudinal domain while this period was absent from of this domain. This raised the possible interpretation that the active regions emerging within the AL are anchored at the bottom of the convective zone where this period was also detected by Howe et al. (2000) and the rest of the active regions emerge from higher layers.

This interpretation offers a feasible explanation for a long enigma, the unknown connections between various space physics processes varying with a period of 1.3 years. The first report about this period was presented by Silverman & Shapiro (1983). They detected the 1.3-year period in century-long visual aurora observations and they admitted that the source of this behavior was unknown. This was followed by a series of reports on this period in different space parameters: solar wind velocity (Richardson et al. 1994; Mursula & Vilppola 2004), solar wind velocity and geomagnetic activity (Paularena

et al. 1995; Mursula & Zieger 2000), B_z component of the interplanetary magnetic field (Szabo et al. 1995), cosmic-ray intensity (Kudela et al. 2002; Singh et al. 2012), and geomagnetic activity (Střeštík 2009); Diaz-Sandoval et al. (2011) refer to this period even in biological phenomena. The most recent overview and analysis of this period in various space physics processes was published by Cho et al. (2013).

The results of Howe et al. (2000) also motivated the search for this period among solar phenomena. Komm et al. (2003) corroborated these results. Krivova & Solanki (2002) found the 1.3-year period in wavelet spectra of sunspot numbers and areas without regard to its spatial relations. Obridko & Shelting (2007) identified this period in the variation of the large-scale magnetic field by combining recent magnetograms and earlier H-alpha filament observations, the resulting time interval covered eight solar cycles. Ruzmaikin et al. (2008) used longitudinally averaged synoptic magnetograms and detected this period too. As an important chain between the solar and interplanetary/geomagnetic phenomena, the period has also been pointed out in the time series of the flare index (Özgüç et al. 2003).

It is a common feature of the above studies that the 1.3-year period is considered as a global feature, its localization on the solar surface is, however, not addressed. However, Paper I presented this localization. The period can be detected in the variation of the flux emergence within the identified AL while it is absent elsewhere. This promises a more direct chain between the dynamics of the tachocline zone and the surface as well as that of the interplanetary space.

The aim of the present work is to specify the spatial and temporal characteristics of the flare activity in connection with the behavior of the AL presented in Paper I.

2. DATABASES OF FLARES AND SUNSPOTS

The Debrecen Photoheliographic Data sunspot catalog[3] (DPD, provided by the Debrecen Heliophysical Observatory; Győri et al. 2011) is used for determining the AL. The DPD is based on white-light images of sunspot groups starting in 1974, so this study can cover 540 CR which roughly equals five solar cycles. The time resolution of the sample is one observation for each day. The catalog provides us with information about the following properties of every sunspot of sunspot groups: the date of observation, the position of the spot and umbra, and the whole spot area. The estimated mean accuracy of the position data is 0.1–0.2 heliographic degrees and the estimated mean precision of the area measure is 10%–20%. For that reason, this data set could probably provide a very detailed sunspot survey; hence, it is suitable to reveal the properties of the longitudinal distribution of the sunspot groups.

We used two solar flare databases. The first data set was taken from the *Geostationary Operational Environmental Satellite* system[4] (*GOES*) starting in 1976. The flare catalog contains information about the date, position of the eruption, the associated active region and the classification code (measured in W m^{-2}), which can be of types A, B, C, M, or X according to the peak flux of the solar flare observed in the 0.1 and 0.8 nm wavelength range. The most energetic class consists of the X-type flares with fluxes in excess of 10^{-4} W m^{-2} at Earth.

Another source of data was the observations by the *Reuven Ramaty High Energy Solar Spectroscopic Imager*[5] (*RHESSI*) satellite (Lin et al. 2002), containing data since 2002. The data set currently contains more than 100,000 events in the energy band from soft-X-ray to gamma-ray. The flare catalog provides the following information for each candidate: dates of explosions, durations, peak intensities, and total count of the number of X-ray photons during the flare event, energy channel of the maximal energy at which the flare is still measurable, location on the solar disk, and quality flags. Based on the positions of certain eruptions, we added associated active regions by using DPD where the *RHESSI* flare list has not contained it. This satellite is able to observe less intense events than the *GOES* satellite. The *RHESSI* flares are mostly micro-flares of *GOES* classes A, B, or C. The most frequent type of *RHESSI* flare is *GOES* class B.

3. THE METHOD OF TRACKING AL

The present investigation began with a similar method as that in Paper I. The areas and positions of all sunspot groups were considered at the time of their maximum area, the solar surface has been divided into longitudinal bins with a width of 20°. The areas of all groups were summed up in each bin (A_i) and normalized by the summarized sunspot group area from the whole surface. Then, the longitudinal activity concentration is represented by the quantity

$$W_{i,\mathrm{CR}} = \frac{A_{i,\mathrm{CR}}}{\sum_{j=1}^{18} A_{j,\mathrm{CR}}}. \quad (1)$$

In every CR, the histogram of the quantity $W_{i,\mathrm{CR}}$ was determined and the significance level estimated (set by 3σ) to filter out the unnecessary noise. The novelty of the present method is that all of the quantities $W_{i,\mathrm{CR}}$ have been omitted in the further statistics that were lower than the previously mentioned limit. Figure 1 shows an example of the histogram of the quantity W in CR 1718. By filtering the data with this limit, 53% of the CRs shows exactly one significant longitudinal belt; meanwhile, the remaining fraction of the data did not show strong in-homogeneous properties.

Many studies have adressed the existence of the co-dominant longitude that has a phase shift of 180° from the dominant peak (Usoskin et al. 2005; Zhang et al. 2007, 2011a). However, we have found that the secondary AL is not, or is hardly detectable, after applying a high-pass filter to sort out the insignificant peaks. For example, by setting the significance level to 2σ, only 23% of the CRs have some sort of double AL distribution. For that reason, the activity at the co-dominant longitude is considered weak and rare, therefore we neglect it in this study.

In Figure 2, we present an example of the steps of the identification method of the AL. There are three panels. The first panel, indicated by letter A, is the surface map of the parameter W. The horizontal x-axis is the time interval between CRs 1700 and 1800. The vertical axis is the longitude in the heliographic coordinate system. Panel (A) shows the first step of our AL tracking method where all of W_i are visible in a certain CR. In the y-axis the 360° solar circumference has been repeated, similarly to Juckett (2006), in order to follow the

[3] http://fenyi.solarobs.unideb.hu/DPD/index.html
[4] http://www.ngdc.noaa.gov/stp/satellite/goes/
[5] http://hesperia.gsfc.nasa.gov/hessidata/dbase/

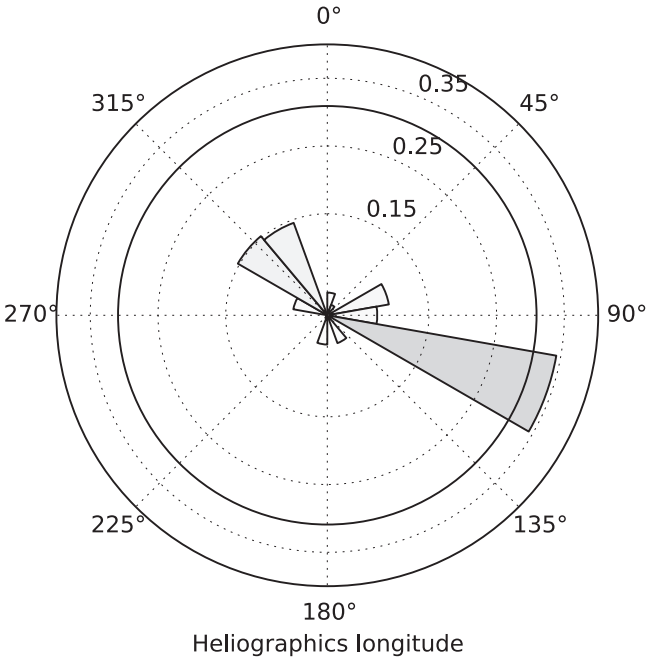

Figure 1. Example for the spatial distribution of the quantity W in the CR 1718. The black line represents the 3σ significance limit. The largest peak represents the AL. In this CR, at the other side (roughly 180° phase shift), the weaker and more disperse peaks correspond to the co-dominant AL.

occasional shifts of the domains of enhanced sunspot activity in the Carrington system. The values of the parameter W are represented by the color of a certain box. $W_{i,\mathrm{CR}} = 1$ is associated with black and $W_{i,\mathrm{CR}} = 0$ is plotted in white.

For further analysis, the Carrington longitudes will now be transformed into units of Carrington phase:

$$\psi = \lambda/360^\circ. \tag{2}$$

Here, the value λ is the longitudinal position in the Heliographic coordinate system; therefore, the ψ values must always be between 0 and 1 (which represents the entire circumference). Please note that the precision of the position of the DPD catalog is about 0.1 heliographic degrees, for that reason, the accuracy of the Carrington phase is about $\pm 2.7 \times 10^{-4}$, which is negligible.

Panel (B) of Figure 2 shows the temporal variation of the Carrington phase. Here, the high-pass filter has been applied (set by 3σ) to filter out the values of parameter W has been omitted, which were lower than 3σ. The significant migration path is more remarkable here.

The final step of the AL tracking method is visualized in panel (C) of Figure 2. We applied a moving average method for smoothing the data. The time-step is 1 CR and the width of the time window is 3 CRs. The repetitions of the AL shifted with one Carrington phase are removed. A phase jump occurs in the case in which the migration of AL enters to the next solar circumference. A phase jump occurs when

$$\delta\phi > \delta\phi^*, \tag{3}$$

where the parameters $\delta\phi$ and $\delta\phi^*$ are defined as

$$\begin{aligned} \delta\phi &= |\psi_{\mathrm{CR}+1} - \psi_{\mathrm{CR}}| \\ \delta\phi^* &= |(\psi_{\mathrm{CR}+1} + \gamma) - \psi_{\mathrm{CR}}|, \end{aligned} \tag{4}$$

and γ is the phase shift, which could be either 1 or -1.

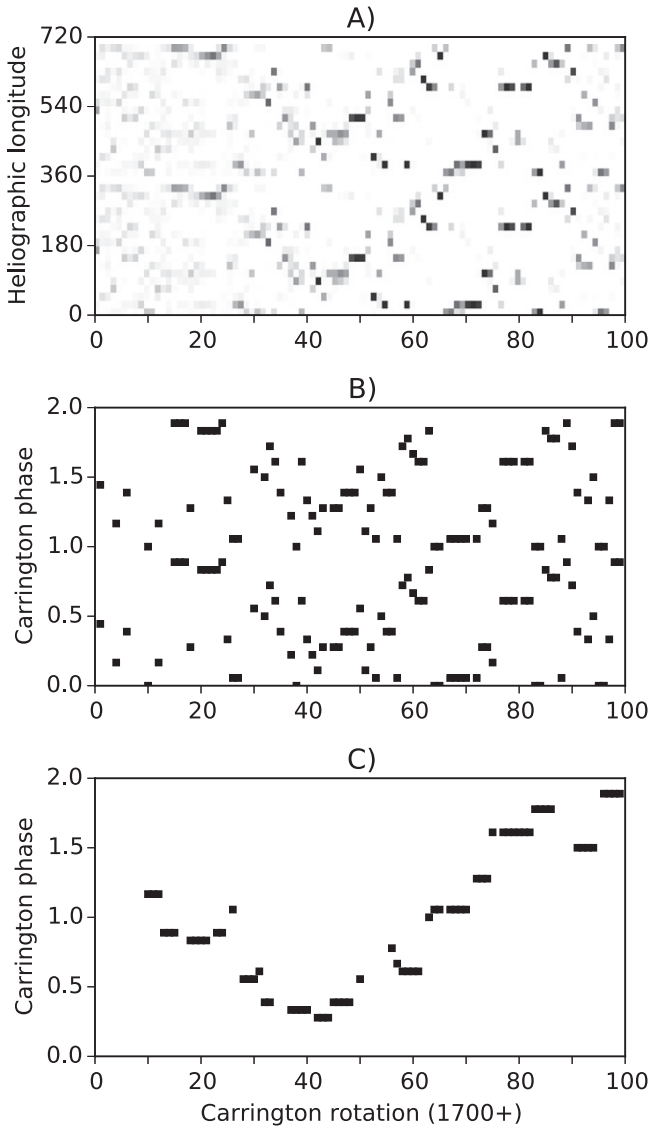

Figure 2. Different stages of the AL finding method. Panel (A) shows the values of parameter W in longitudinal bins of 20° and temporal bins of 1 CR. The darker marker indicates a larger value of W. Panel (B) shows the Carrington phase of W vs. time after applying a 3σ high-pass filter to omit all of the bins with an insignificant value of W. Panel (C) shows the final stage of the finding method of AL. The repetition of the pattern in Carrington phases are removed and 3-CR moving average has been applied to the remaining peaks of W. The result shows the migration path of AL.

For instance, a phase jump can be seen in Figure 2 in CR 1765 when the curve is crossing from Phase 0–1 to Phase 1–2. The shape of the migration path may depend on how the phase jumps are handled. Although the long-term trends of the migration path may not always be well determined because of the phase jumps and the scatter of the points around it, this may hardly affect the statistical results based on the distances measured from the actual AL values. Thus, the distances from AL are used in the next sections.

4. TRACKING AL IN THE DPD ERA

The AL tracking method was applied to the entire DPD-era, containing 540 CRs from CR 1610 to CR 2150. The indicated time interval consists of three full (namely Cycles 21, 22, and 23) and two partially visible (namely Cycles 20 and 24) solar

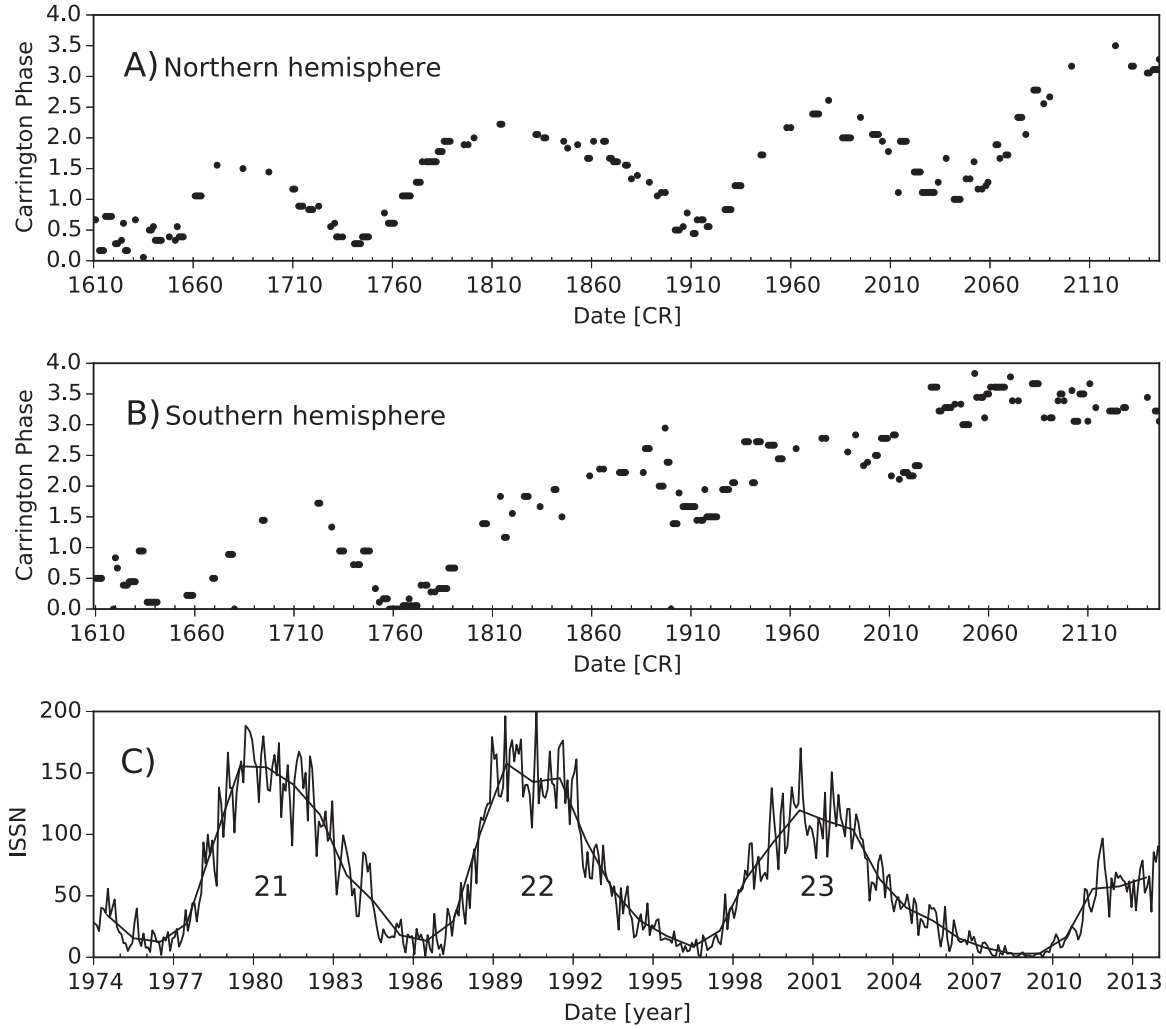

Figure 3. Activity maps for whole the DPD-era (1974–2014). Panel (A) shows the migration of the AL on the northern hemisphere. The black markers mean the longitudinal belts of most enhanced sunspot activity (AL) in certain CRs. Panel (B): the same as Panel (A), but for the southern hemisphere. Panel (C) represents the temporal variation of the International Sunspot Number (ISSN). The numbers of the solar cycles are also marked.

cycles. The two hemispheres are treated separately. Sunspot groups were selected within a longitudinal distance of $\pm 75^{\circ}$ from the central meridian in order to avoid the less accurate area and position estimates at the limb. In Figure 3, we plot the temporal variation of the Carrington phase for the northern hemisphere (Panel (A)) and the southern hemisphere (Panel (B)). Panel (C) shows the temporal variation of the International Sunspot Number provided by the SIDC-team.[6]

The migration of AL in the northern hemisphere is clearly recognizable. The shape of the migration seems to be a set of parabola with prograde and retrograde phases. On the prograde phase, the angular velocity of the AL is faster than the CR and the retrograde phase, on the contrary; it shows a slower angular velocity. The maxima of parabola-like curves roughly correspond to the maxima of solar cycles, but the beginnings and ends of the pro- and retrograde phases do not correspond to the minima of the solar cycles. In Cycles 21 and 23, the retrograde and prograde parts of the parabola are shorter and the migration shape of the AL of the Cycle 22 clearly shows a longer period in time than the period of the solar cycles. On the southern hemisphere, a similar parabola shape migration pattern has been shown, but the times of minima and times of maxima differ from those of Panel A and they are sometimes less expressed.

The migration of the longitude of enhanced sunspot activity has been found in numerous earlier studies. First, the detection of some patterns of migrating AL of sunspot groups was reported by Berdyugina & Usoskin (2003). Juckett (2006) found a similar returning phase in the time interval between CRs 1720–1750 by using low-degree surface spherical harmonics. The retrograde phase was also observed on a restricted interval by Bumba et al. (2000) for Cycle 22.

In Paper I, we concluded that the migration paths of ALs did not correspond sharply to the shape of the 11-year cycle. This statement was based on two parabolic patterns of AL, one in the northern hemisphere in Cycle 22 and one in the southern hemisphere in Cycle 24. The present extension of the study confirms this statement for the whole interval. Based on these longer time series of migration patterns, it is clearer that the minima of the patterns mostly do not coincide with those of the solar cycles. In addition, the two hemispheres are able to produce different migration patterns with different locations of minima and maxima.

[6] http://www.sidc.be/silso/datafiles

For this reason, differential rotation can hardly be involved in the migration of AL. Balthasar (2007) did not find signatures of differential rotation either, similarly to the above-mentioned works of Juckett (2006, 2007). Furthermore, note that the AL does not always seem to be identifiable. 47% of the data did not show significantly enhanced longitudinal activity in the case of the 3σ significance limit.

5. SPATIAL DISTRIBUTION OF SOLAR FLARE OCCURRENCE

In this section, we investigate the relationship between the position of solar flares (the data are taken by the *GOES* and *RHESSI* satellites) and the longitude of enhanced sunspot activity (AL). For that reason, a new parameter is defined that is the shortest longitudinal distance between the position of the AL and the position of a certain event. The phase difference is defined by

$$\delta\psi = |\mathrm{AL_{CR}} - L_{\mathrm{CR}}|. \quad (5)$$

Here, L_{CR} is the longitudinal position of the *RHESSI* and *GOES* observations in Carrington phases. $\mathrm{AL_{CR}}$ represents the position of the AL defined in Section 4. The parameter $\delta\psi$ is reduced by a unit phase if it is larger than 0.5 because the distance cannot be larger than 180°. $\delta\psi = 0$ means that the flare is located at the AL; $\delta\psi = 0.5$ means that the flare is located on the other side of the Sun opposite the AL.

Figure 4 contains three plots where panels (A) and (B) show the spatial distribution of the *RHESSI* and *GOES* flares with respect to the AL (the position of the AL corresponds to $\delta\psi = 0$). The gray area represents the frequency distribution normalized by the sample number. On the plots, there is only one significant peak for each statistic and after that a long plateau with insignificant local peaks. The significance limit was defined by the standard deviation of the sample ($\sigma_{\mathrm{GOES}} = 9.8$ and $\sigma_{\mathrm{RHESSI}} = 10.5$). The distributions show that most of the solar flares are concentrated in a relatively narrow longitudinal zone. In Paper I, we found that the AL of sunspot groups is as narrow as 20°–30°. Here, the spatial distribution of solar flares shows similar behavior. To estimate the quantitative properties of this distribution, different models have been tested and the exponential distribution has provided a good enough result for each data set. The best exponential models are indicated by the solid line in panel (A) and by the dashed line in panel (B).

We defined control groups where the position of the AL was generated by random numbers. This test was inspired by Pelt et al. (2005) who criticized the AL identification method of Berdyugina & Usoskin (2003). Pelt et al. (2005) reconstructed the distribution of the AL with random sunspot longitudes. For that reason, we repeated the statistical study by using the identification of the AL based on random longitudinal sunspot positions. The result of the control group does not show significant peaks, thus it can be represented by the dotted line of homogeneous distribution in Figure 4. This means that our AL identification method does not cause false significant peaks, which would affect the results of the study of in-homogeneous longitudinal properties.

Panel (C) of Figure 4 shows the cumulative distribution of the spatial distributions. The solid and dashed lines (based on *GOES* and *RHESSI* observations) have a steep increasing phase between the values of 0 and 0.1 after the functions

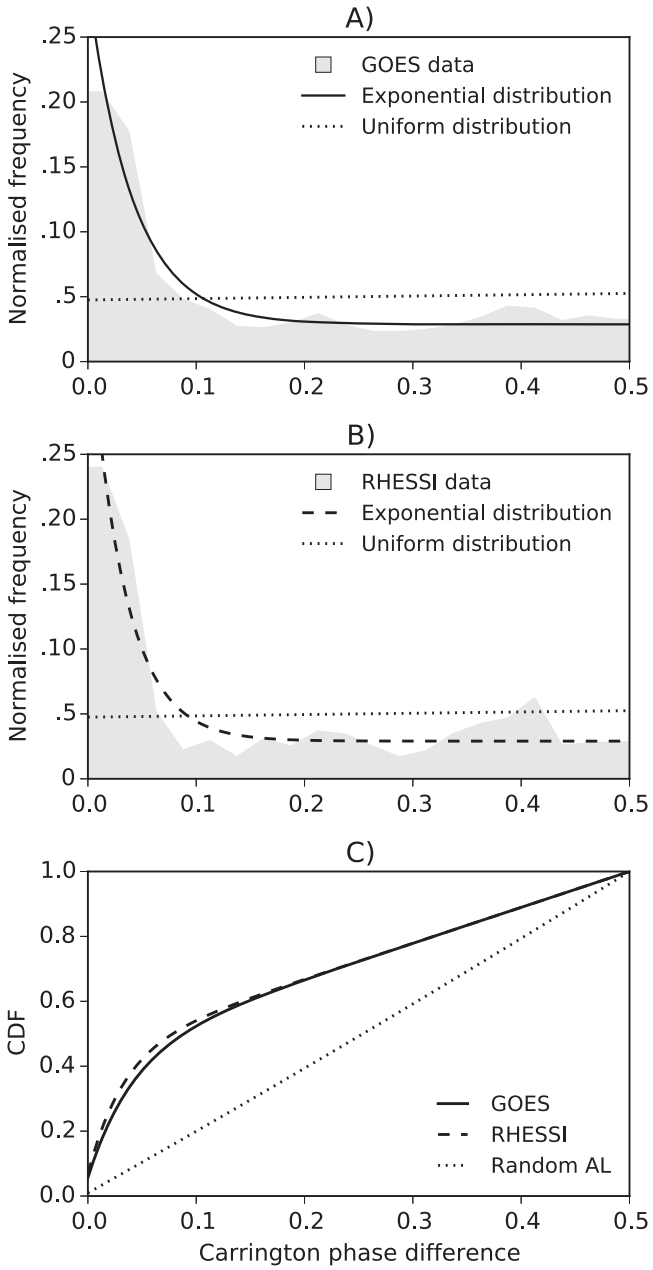

Figure 4. Spatial distributions of the parameter $\delta\psi$. Panel (A) shows the spatial distribution of *GOES* flares with respect to the AL, represented by the gray area. The solid line is the fitted exponential model distribution and the dotted line means the uniform distribution based on random AL. Panel (B) represents the same statistics, but the *RHESSI* flare list has been used. The dashed line is the fitted exponential model distribution and the dotted line means the uniform distribution based on random AL. The last figure (Panel (C)) shows the cumulative distribution of the fitted model distributions.

show a constantly less steep increasing trend. These models allow us to estimate that most of the solar flares (around 60%) occur in the longitudinal zone of ±36° around the position of AL. The dotted line is the cumulative distribution of the uniform distribution based on random longitudinal positions. In this distribution, the mentioned longitudinal domain would only contain 20% of the solar flares. This means that the AL plays a significant role in the spatial distribution of flare occurrences.

6. TEMPORAL PROPERTIES OF SOLAR FLARES NEAR AL

The aim of this section is to reveal the temporal properties of the occurrence of solar flares located near to the AL. We showed in the previous section that most of the solar flares detected by the *RHESSI* and *GOES* satellite are concentrated in a longitudinal strip of 0.1 Carrington phase width around the AL. Here, we focus only on this specific region. We omit all of the solar flares that occur further than the 0.1 Carrington phase. This spatial limit corresponds to a neighborhood of $\pm 36^\circ$ of the dominant AL in the Carrington coordinate system.

In every CR, we summed up the number of all *GOES* and *RHESSI* flares and the two hemispheres are distinguished. The parameter *dN* is defined for this statistic:

$$dN = N_{\mathrm{CR}} - N_{\mathrm{CR}+1}. \quad (6)$$

In Figure 5, the results of the statistics are plotted for data provided by the *GOES* satellite. The first (northern hemisphere) and third (southern hemisphere) panels are the temporal variations of the parameter *dN*. The time series is smoothed by the moving average method with 4-CR smoothing window and 1-CR step. Below each plot, the wavelet spectra or the parameter *dN* are presented. All of the flares are taken into account for both statistics.

In the *GOES*-era four significant periods (confidence levels set by 95%) and several clearly visible, but not significant, peaks are found on both hemispheres. In the northern hemisphere (NH) during Cycle 21 (CR1710—CR1750) there is a fluctuation with a 18–24 CR period (indicated by the entire range of the red contour). The same period is found in Cycle 22 (CR1810-CR1750). This fluctuation corresponds to 1.3–1.8 years. There is one more significant fluctuation in Cycle 22 with about 11–13 CRs, which corresponds to a 0.8–1 year fluctuation period. The same period is also found in Cycles 21 and 23 but the power of the peaks are below the 95% confidence level. In the southern hemisphere (SH), only one significant peak is found in Cycle 22. The period is 14–16 CR (1–1.2 years). This period is also visible, below the CI 95%, in Cycles 21 and 23.

Figure 6 shows a similar statistic for the data taken from the *RHESSI* catalog. The *RHESSI*-era starts in 2002 hence only Cycles 23 and 24 are covered. In the northern hemisphere, one significant period can be seen, corresponding to 0.6–0.7 years in Cycle 24 (2105CR–2120CR). The periods of 0.8 and 1.3 years are also weakly visible in Cycles 23 and 24 but the powers of the fluctuations are, again, under the 95% confidence level. In the southern hemisphere, only one peak is visible in Cycle 24. The period is around 1.3 years but, unfortunately, this peak is within the COI. The last two rows of Table 1 only contain *RHESSI* data about a period of 0.6–0.7 years, but this period was not detectable in the *GOES* measurements. Because of this contradiction in this time interval the suspected connection of surface activity with the dynamics of the tachocline layer probably does not work. The significant periods found are summarized in Table 1.

7. DISCUSSION AND CONCLUSION

Zhang et al. (2008) found that the ALs with half widths of 20°–30° contain 80% of C-flares during the solar minimum and X-flares during solar maximum. The AL was defined by the dynamic reference frame, introduced by Usoskin et al. (2005). Hence, their study assumes two detectable and equally strong

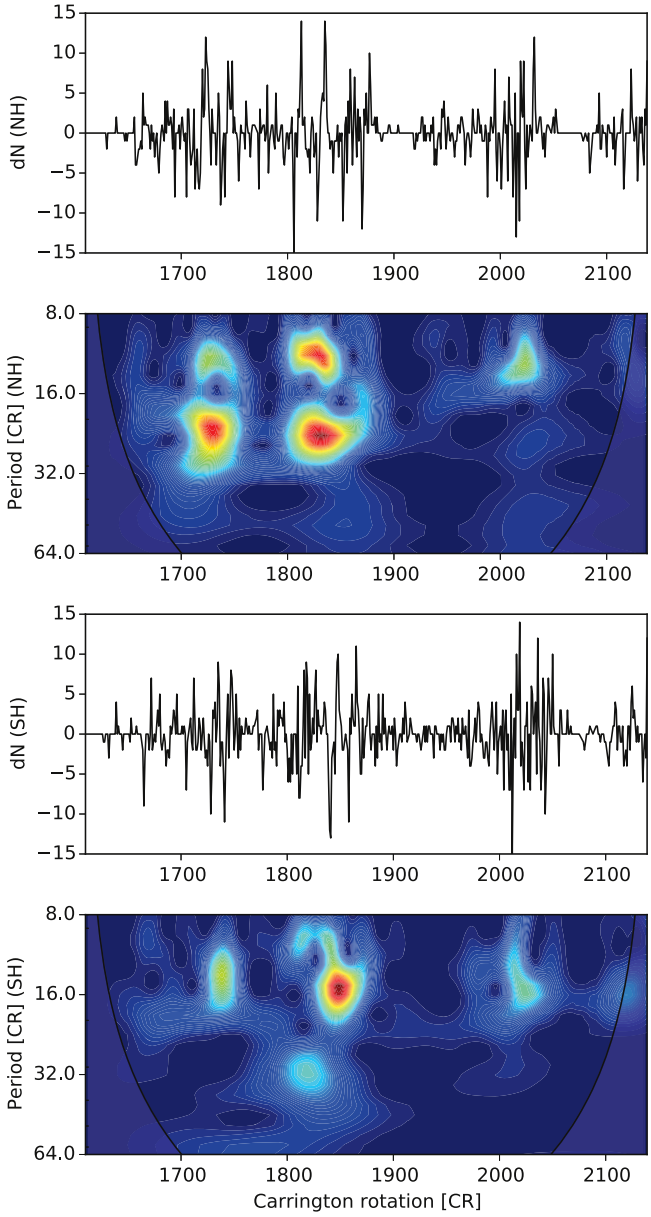

Figure 5. Temporal distribution of the solar flares near to the dominant AL. The smoothed solid black lines of the first and the third subplots indicate the time variation of the *GOES* solar flare variance. Below those plots, continuous wavelet transforms of the time series are presented. The first and the second subplots contain data from the northern hemisphere (NH) and the last two subplots show the southern hemisphere (SH). The bottom axis is time in CR for each subplot. The red contours enclose regions of greater than 95% confidence. The gray faded regions on either end of the figures indicate the cone of influence (COI) where the edge effect becomes significant. For that reason, all of the found peaks under the COI has been omitted.

ALs, separated by 180°. In our study, however, the secondary AL was found to be weak in comparison with the primary one. Our results imply that only the primary belt contains 60% of all solar flares. The entire width of the belt is $\pm 36^\circ$. Both values correspond well to the results, investigated by Huang et al. (2013) who calculated the ratio between the number of flaring active regions and the total number of active regions. The active region that is near the AL is prone to erupt. The active region that is far away from the AL produces solar flares with little probability.

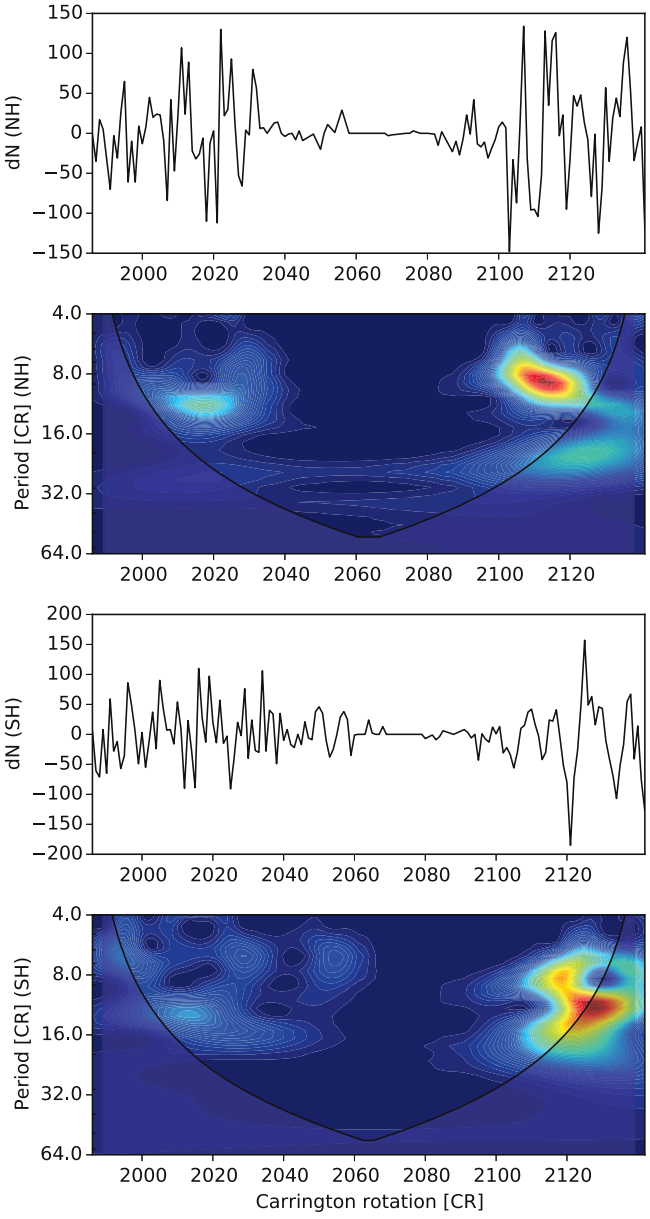

Figure 6. Same statistics as in Figure 6, but the data was taken from the *RHESSI* catalog. The bottom axis is time in CR. The indicated period covers the whole *RHESSI* database from 2002. The meaning of the color codes are the same, the red contour encloses regions of greater than 95% confidence. The gray faded regions on either end of the figures indicate the cone of influence (COI) where the edge effect become significant for that reason all of the found peaks under the COI has been omitted.

Table 1
Significant Periods (CI 95%) Obtained by Wavelet Analysis Based on the Time Series of the Parameter *dN*

Time (CR)	Period (CR)	Period (year)	Hemi	Source
1710–1750	18–24	1.3–1.8	NH	*GOES*
1810–1850	18–24	1.3–1.8	NH	*GOES*
1810–1850	11–13	0.8–1.0	NH	*GOES*
1850–1870	14–16	1.0–1.2	SH	*GOES*
2105–2120	8–10	0.6–0.7	NH	*RHESSI*
2115–2120	8–10	0.6–0.7	SH	*RHESSI*

Numerous earlier studies reported periods between one and two years in a number of heliospheric parameters such as the interplanetary magnetic field (Vilppola & Mursula 2001), the solar wind speed (Mursula et al. 2002), the cosmic rays, the geomagnetic activity (Paularena et al. 1995), the coronal index, and the 10.7 cm solar flux data (Forgács-Dajka & Borkovits 2007). Mursula et al. (2002) found mid-term quasi-periodicities based on the "aa" index of global geomagnetic activity. Periods found correspond to 1.2–1.4 years and a slightly longer period of about 1.5–1.7 years. Cho et al. (2013) found significant signals of 1.3 years between 1987 and 1995 in the solar wind speed, IMF B_z, geomagnetic aa index, and ap index, as well as in the tachocline layer $\Delta\Omega$ after 1997.

The 1.3-year period of flare emergence in the AL found here corresponds well with our previously found 1.3-year period of spot emergence. It has been shown in Paper I that this period can only be detected in a narrow belt of 30° along the parabola-shaped path of AL, but it is absent, or overwhelmed, in the entire material. The presence of the ∼1.3-year period within the active belt allows the conjecture that the ALs may be connected to a source region close to the tachocline zone. This implication is based on the results by Howe et al. (2000), who found the same period of the radial torsional oscillation at the tachocline zone during the period between 1995 and 2000 and by Bigazzi & Ruzmaikin (2004), who argued that the non-axisymmetry of the solar dynamo could only remain at the bottom of the convective zone.

It may be interesting to investigate whether the 1.3-year fluctuations in the tachocline zone and the interplanetary phenomena may be connected. It could be possible because the oscillation of the tachocline zone, the flux emergence of the AL, and the flare occurrence within the AL show similar temporal properties. However, to reveal this connection is not an easy task because on the one hand the time intervals of their observations are not continuously overlapped. On the other hand this fluctuation is not always present in any of these regions.

For the period between 1995 and 2000, Paper I also presented a clear signature of the 1.3-year fluctuation in the magnetic flux emergence within the AL, the targeted time interval has a short overlap with that studied by Howe et al. (2000). The first two intervals in Table I are also parts of this interval and they also contain the 1.3-year periodicity of flaring activity. Thus, in spite of the incomplete observational coverage, it can be assumed that the excitation of the fluctuation at the tachocline layer may be connected to the dynamics of flux emergence in the AL and with the fluctuation of the flaring activity and interplanetary impact. The temporal variation of the number of solar flares could be related to the flux emergence based on the simple idea that the probability of a flare occurrence is higher if there is an increased number of active regions. However, there is an uncertainty as to why the different hemispheres could produce different fluctuations. This question definitely needs further study.

Howe et al. (2011) concluded that the significance of the 1.3-year fluctuation became less significant between 2000 and 2010 and at the end of the indicated time period the 1.3-year fluctuation has not found. There are no results published after 2010. However, after 2000, we have also not detected this period in the flaring activity or in the temporal properties of the sunspot flux emergence (Paper I).

8. SUMMARY

Many flare prediction models employ the properties of active regions, such as morphological information, area, or the magnetic field of sunspot groups. The spatial distribution of active regions has not been used widely, such as longitudinal distribution. If we assume the most flare-productive active regions tend to be located in or close to the active longitudinal belt, then this may allow us to predict the geo-effective position of the domain of enhanced flaring probability for a couple of months or years ahead. In this paper, we studied the spatial and temporal properties of solar flares based on observations of the *GOES* and *RHESSI* satellites.

We have found that there is a narrow longitudinal belt of considerably enhanced sunspot activity migrating in the time-longitude domain. The migration path is similar to that of a series of parabolic shape curves. A parabola-like section of the migration path does not follow the solar cycle and it has fluctuating temporal properties. The co-dominant longitudinal belt, phase shifted by 180°, is relatively weak in comparison to the main AL. The main AL is not always detectable, but the migration path of the activity is recognizable based on the DPD sunspot data in the time interval between 1974 and 2014.

Our results show that the main AL plays a crucial role in the global position of solar flare occurrence. Most flare active groups appear in the ±36° width of the AL. The temporal variation of the number of solar flare shows fluctuations of 0.8, 1.3, and 1.8 years within the active longitudinal belt. This temporal distribution may also provide an improved flare forecasting opportunity.

N.G. is thankful for the invitation, support, and hospitality received from Kalevi Mursula (Department of Physical Sciences, University of Oulu, Finland). The research leading to these results has received funding from the European Community's Seventh Framework Programme (FP7/2007–2013) under grant agreement eHEROES (project No. 284461). This research has made use of SunPy, an open-source and free community-developed Python solar data analysis package (Mumford et al. 2013). Finally, N.G. is thankful for the support received from the University of Sheffield.

REFERENCES

Bai, T. 1987, ApJ, 314, 795
Bai, T. 1988, ApJ, 328, 860
Bai, T. 2003, ApJ, 585, 1114
Balthasar, H. 2007, A&A, 471, 281
Balthasar, H., & Schüssler, M. 1983, SoPh, 87, 23
Becker, U. 1955, Z. Astrophys., 37, 47
Berdyugina, S. V., & Usoskin, I. G. 2003, A&A, 405, 1121
Bigazzi, A., & Ruzmaikin, A. 2004, ApJ., 604, 944
Brouwer, M. P., & Zwaan, C. 1990, SoPh, 129, 221
Bumba, V., Garcia, A., & Klvaňa, M. 2000, SoPh, 196, 403
Carrington, R. C. 1863, in Observations of the Spots on the Sun (London: Redhill, Williams and Norgate), 246
Castenmiller, M. J. M., Zwaan, C., & van der Zalm, E. B. J. 1986, SoPh, 105, 237
Cho, I.-H., Hwang, J., & Park, Y.-D. 2013, SoPh, 289, 707
Diaz-Sandoval, R., Erdelyi, R., & Maheswaran, R. 2011, AnGp, 29, 1
Forgács-Dajka, E., & Borkovits, T. 2007, MNRAS, 374, 282
Gyenge, N., Baranyi, T., & Ludmány, A. 2014, SoPh, 289, 579 Paper I
Győri, L., Baranyi, T., & Ludmány, A. 2011, in Proc. IAU Symp. 273, The Physics of Sun and Star Spots, ed. D. Choudhary & K. Strassmeier (Cambridge: Cambridge Univ. Press), 403
Henney, C. J., & Durney, B. R. 2005, ASPC, 346, 381
Howe, R., Christensen-Dalsgaard, J., Hill, F., et al. 2000, Sci, 287, 2456
Howe, R., Komm, R., Hill, F., et al. 2011, JPhCS, 271, 012075
Huang, X., Zhang, L., Wang, H., & Li, L. 2013, A&A, 549, 6
Ivanov, E. V. 2007, AdSpR, 40, 959
Juckett, D. A. 2006, SoPh, 245, 37
Juckett, D. A. 2007, SoPh, 245, 37
Kitchatinov, L. L., & Olemskoy, S. V. 2005, AstL, 31, 280
Komm, R., Howe, R., Durney, B. R., & Hill, F. 2003, ApJ, 586, 650
Krivova, N. A., & Solanki, S. K. 2002, A&A, 394, 701
Kudela, K., Rybák, J., Antalová, A., & Storini, M. 2002, SoPh, 205, 165
Lin, R. P., Dennis, B. R., Hurford, G. J., et al. 2002, SoPh, 210, 3
Losh, H. M. 1939, Publ.Obs.Michigan, 7, 127
Maunder, E. W. 1905, MNRAS, 65, 538
Mumford, S., Christe, S., Pérez-Suárez, D., et al. 2015, CS&D, 8, 014009
Mursula, K., & Vilppola, J. H. 2004, SoPh, 221, 337
Mursula, K., & Zieger, B. 2000, AdSpR, 25, 1939
Mursula, K., Zieger, B., & Vilppola, J. H. 2002, SoPh, 212, 201
Obridko, V. N., & Shelting, B. D. 2007, AdSpR, 40, 1006
Özgüç, A., Ataç, T., & Rybák, J. 2003, SoPh, 214, 375
Paularena, K. I., Szabo, A., & Richardson, J. D. 1995, GeoRL, 22, 3001
Pelt, J., Tuominen, I., & Brooke, J. 2005, A&A, 429, 1093
Richardson, J. D., Paularena, K. I., Belcher, J. W., & Lazarus, A. J. 1994, GeoRL, 21, 1559
Ruzmaikin, A., Cadavid, A. C., & Lawrence, J. 2008, JASTP, 70, 2112
Silverman, S. M., & Shapiro, R. 1983, JGR, 88, 6310
Singh, Y. P., Gautam, S., & Badruddin, B. 2012, JASTP, 89, 48
Střeštík, J. 2009, CEJG, 1, 152
Szabo, A., Lepping, R. P., & King, J. H. 1995, GeoRL, 22, 1845
Usoskin, I. G., Berdyugina, S. V., & Poutanen, J. 2005, A&A, 441, 347
Vilppola, J. H., & Mursula, K. 2001, American Geophysical Union
Warwick, C. S. 1965, ApJ, 141, 500
Zhang, L. Y., Mursula, K., Usoskin, I. G., & Wang, H. N. 2011a, A&A, 529, 23
Zhang, L. Y., Mursula, K., Usoskin, I. G., & Wang, H. N. 2011b, JASTP, 73, 258
Zhang, L. Y., Wang, H. N., & Du, Z. L. 2008, A&A, 484, 523
Zhang, L. Y., Wang, H. N., Du, Z. L., Cui, Y. M., & He, H. 2007, A&A, 471, 711